Tectonophysics 503 (2011) 195–200

Contents lists available at ScienceDirect

Tectonophysics

journal homepage: www.elsevier.com/locate/tecto

Reactivation tendency analysis: A theory for predicting the temporal evolution of preexisting weakness under uniform stress state

Hengmao Tong [a], An Yin [b,c,*]

[a] State Key Laboratory of Petroleum Resources and Prospecting, China University of Petroleum, Beijing 102249, China
[b] Department of Earth and Space Sciences and Institute of Geophysics and Planetary Physics, University of California, Los Angeles, CA 90095–1567, USA
[c] Structural Geology Group, School of Earth Sciences and Resources, China University of Geosciences, Beijing 100083, China

ARTICLE INFO

Article history:
Received 16 February 2011
Received in revised form 23 February 2011
Accepted 25 February 2011
Available online 3 March 2011

Keywords:
Preexisting weakness
Reactivation
Mohr space
Sandbox experiment

ABSTRACT

Understanding the mechanical controls on reactivation of preexisting weakness is a fundamental problem in tectonic studies. In this study, we develop a theoretical framework for evaluating the likelihood of seismicity on active faults and the sequence of reactivation of multiple sets of preexisting weakness. Our analysis overcomes the restrictions of the early work that assumes uniform coefficient of friction across all preexisting planes with negligible cohesive strength and vertical or horizontal orientations of principal stresses. Using a coordinate-system transformation, we developed a new graphical technique that can express the reactivation problem in the Mohr space with the principal stresses oriented neither vertically nor horizontally. We verified the predicted sequence of reactivation on preexisting weakness and initiation of new fractures, according to the Byerlee law and the Coulomb fracture criterion, by conducting a simple sandbox experiment. Our proposed reactivation-tendency analysis can be expanded to evaluate the likelihood of seismicity on a single fault with curvi-planar geometry (e.g., listric normal faults, ramp-flat thrusts, and strike-slip faults with restraining- and releasing-bend geometry). Our analysis also provides a new insight into the mechanical cause of temporal evolution of pre-existing weakness in geologic records. Finally, our work implies that the sequence of faulting reactivated from preexisting weakness provides critical information on the mechanical properties of the deforming lithosphere.

1. Introduction

Understanding the mechanical controls on reactivation of preexisting weakness is a fundamental problem in the studies of lithospheric deformation (e.g., Agostini et al., 2009; Donath, 1961; Dyksterhuis and Muller, 2008; McKenzie, 1969; Sokoutis et al., 2007). Morris et al. (1996) pioneered the concept of slip-tendency analysis for evaluating the likelihood of reactivation of multiple preexisting planes under a uniform stress state. This method has since been widely used to evaluate seismic risks in actively deforming regions or areas experiencing drastic changes in pore-fluid pressures due to pumping and withdrawal of groundwater that had affected the local state of stress (e.g., Bailey and Ben-Zion, 2009; Geza et al., 2004, 2005; Loïc et al., 2008; Moeck et al., 2009; Wesnousky, 1999). The theoretical framework for slip-tendency analysis is based on the following three assumptions: (1) the coefficient of friction is the same on all preexisting planes, (2) the principal stresses are vertical or horizontal, and (3) the cohesive strength on preexisting planes is negligible. These assumptions have limited the general usage of this innovative approach in evaluating earthquake potentials among active faults. First, the coefficient of friction may vary significantly from fault to fault or from one preexisting weakness plane to another (e.g., clay is much weaker than most other rock types) (Byerlee, 1978). Second, the principal stresses may rotate from the vertical and horizontal directions in the brittle upper crust, possibly due to pluton emplacement, ductile flow, and shearing on low-angle faults from below (e.g., Melosh, 1990; Spencer and Chase, 1989; Yin, 1989; Yin and Kelty, 2000). Third, cohesive strength on preexisting weak planes could be appreciable due to crack healing. As the healing process is time-dependent, the cohesive strength must vary considerably from one weak plane to the other (Li et al., 2003; Vidale and Li, 2003). This study expands the work of Morris et al. (1996) by presenting a general model for evaluating reactivation tendency for preexisting weak planes.

2. Mechanical model

In a region with the presence of preexisting weak planes under a uniform stress state, two types of shear failure may occur: (1) fracturing of coherent rock according to the Coulomb fracture criterion, and (2) shear failure of preexisting planes according to the Byerlee's law:

$$\tau_{nC} = C + \mu_C \sigma_{nC} \tag{1a}$$

$$\tau^j_{nW} = C^j_W + \mu^j_W \sigma^j_{nW} \tag{1b}$$

* Corresponding author. Tel.: +1 310 497 7365; fax: +1 310 825 2779.
E-mail address: yin@ess.ucla.edu (A. Yin).

0040-1951/$ – see front matter © 2011 Elsevier B.V. All rights reserved.
doi:10.1016/j.tecto.2011.02.012

where τ_{nC} and τ^j_{nW} are failure shear stress of coherent rock and preexisting plane, σ_{nC} and σ^j_{nW}, C and C^j_W, and μ_C and μ^j_W are effective normal-stress components, cohesive strengths, and coefficients of friction for the coherent rock and the jth preexisting plane, respectively. Superscript $j=1, 2, 3, \ldots n$, with n equal to the total number of preexisting planes in the region. The effective normal stresses σ_{nC} and σ^j_{nW} are defined as $\sigma_{nC}=(\sigma'_{nC}-p_{fC})$, and $\sigma^j_{nW}=(\sigma'^j_{nW}-p^j_{fW})$, where σ'_{nC} and σ'^j_{nW} are normal-stress components, and p_{fC} and p^j_{fW} are pore-fluid pressure within coherent rock and in the zone of the jth preexisting weak plane in the region under uniform stress. Morris et al. (1996) defined a slip-tendency factor as

$$T^j_S = \frac{\tau^j_n}{\sigma^j_n} \tag{2}$$

where τ^j_n and σ^j_n are shear and effective normal stress on the jth preexisting plane. The likelihood of reactivation of the preexisting plane increases as T_S approaches the coefficient of friction (μ), which is defined as the ratio between the shear failure stress and the corresponding effective normal stress (i.e., τ_n/σ_n). However, the above statement is only valid when the cohesive strength in Byerlee's law can be neglected. When this is not the case, i.e., $T_S=\mu+C/\sigma_n$, the slip-tendency factor is no longer a constant and thus cannot be used to evaluate the likelihood of reactivation of preexisting planes. To avoid this problem, we define a new parameter below, which we refer to as the *reactivation-tendency factor*

$$f^j_R = \frac{\tau_n}{\tau^j_n} = \frac{\tau_n}{C^j_W + \mu^j_W \sigma_n} \tag{3}$$

where τ_n is the shear stress on the jth preexisting plane, τ^j_n is the critical shear stress for frictional failure on the preexisting plane, and σ_n is the effective normal stress on the preexisting plane.

To avoid the assumption that the principal stresses must be horizontal or vertical as assumed in the Morris et al. (1996) analysis, we first consider a preexisting plane in the geographic coordinate ($\boldsymbol{x_1}$, $\boldsymbol{x_2}$, $\boldsymbol{x_3}$) pointing to the north, east, and down directions, respectively (Fig. 1a). The directional cosines of the normal to the

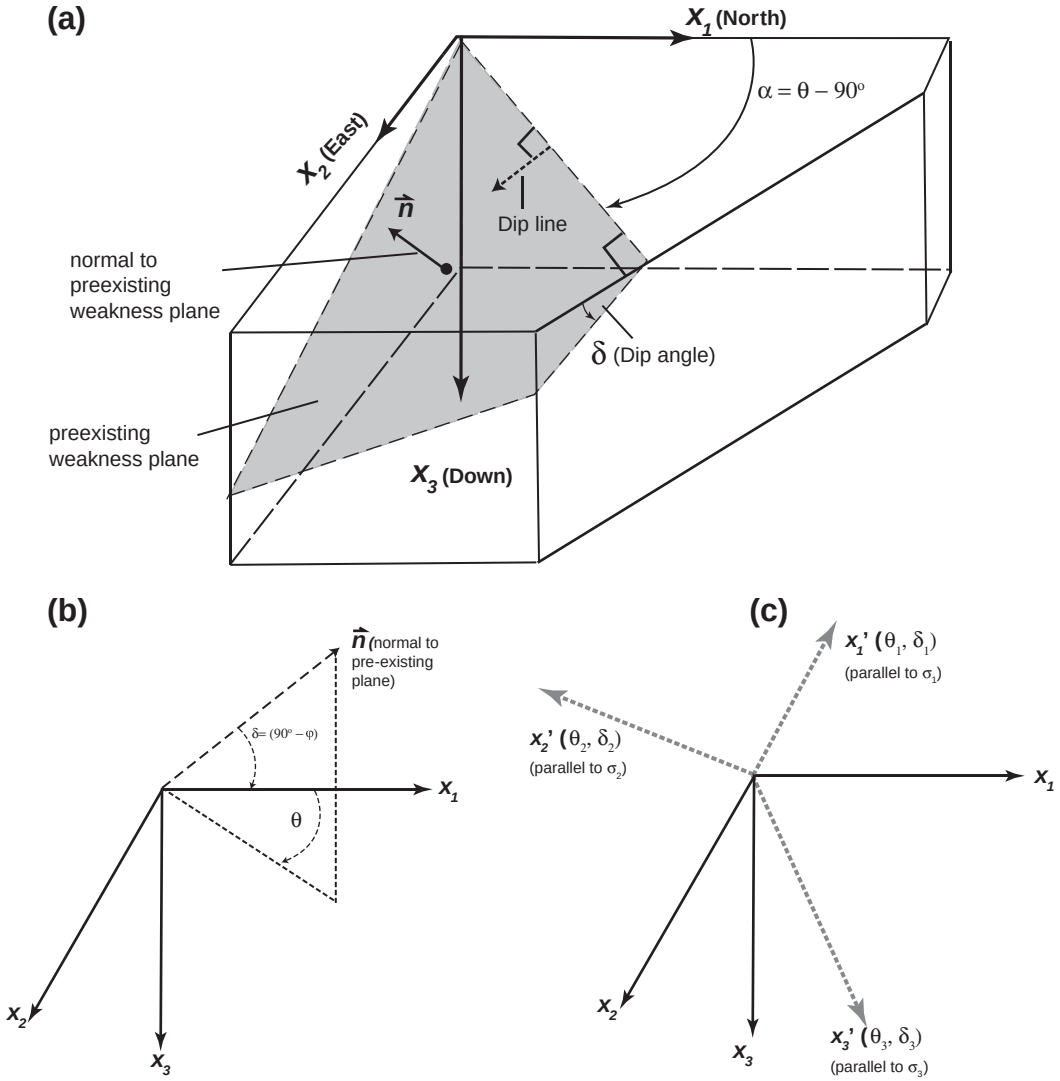

Fig. 1. A preexisting weak plane in a geographic coordinate (x_1, x_2, and x_3), with x_1 pointing down, x_2 pointing north, and x_3 pointing east. Angles θ and φ are the dip direction and dip angle of the preexisting plane and θ, δ is the trend and plunge of its normal; $\delta=90°-\varphi$. The coordinate system (x'_1, x'_2 and x'_3) is constructed by letting x'_1, x'_2 and x'_3 parallel to the principal stresses σ_1, σ_2, and σ_3, respectively. The trend and plunge of the x'_1, x'_2 and x'_3 in the coordinate system (x_1, x_2, and x_3) are (θ_1 and δ_1), (θ_2 and δ_2), and (θ_3 and δ_3), respectively.

preexisting plane, $\boldsymbol{n}=(l_n, m_n, n_n)$, can be related to its dip angle (φ) and the dip direction (θ) by the following relationships (Fig. 1b):

$$\begin{aligned} l_n &= -\cos\varphi \\ m_n &= \sin\varphi\cos\theta \\ n_n &= \sin\varphi\sin\theta. \end{aligned} \tag{4}$$

Similarly, the directional cosines of the effective principal stresses, $\boldsymbol{n_i}=(l_i, m_i, n_i)$, where $i=1$, 2, and 3 for maximum, intermediate, and minimal compressive stresses (σ_1, σ_2, and σ_3) can also be related to their trends and plunges by

$$\begin{aligned} l_i &= -\sin\delta_i \\ mi &= \cos\delta_i\cos\theta_i \\ n_i &= \cos\delta_i\sin\theta_i. \end{aligned} \tag{5}$$

To keep the algebra simple, we assign a new coordinate system in which $\boldsymbol{x'_1}$, $\boldsymbol{x'_2}$, and $\boldsymbol{x'_3}$ are parallel to the directions of σ_1, σ_2, and σ_3 (Fig. 1c). The normal to the preexisting plane in the new coordinate system, $\boldsymbol{n'}=(l'_n, m'_n, n'_n)$, and in the old system, $n=(l_n, m_n, n_n)$, can be exchanged using the matrix operation below:

$$\begin{bmatrix} l'_n \\ m'_n \\ n'_n \end{bmatrix} = \begin{bmatrix} l_1 & m_1 & n_1 \\ l_2 & m_2 & n_2 \\ l_3 & m_3 & n_3 \end{bmatrix} \begin{bmatrix} l_n \\ m_n \\ n_n \end{bmatrix}. \tag{6}$$

In the new coordinate system, the effective normal stress and shear stress σ_n and τ_n on the preexisting plane can be related to the three effective principal stresses and the directional cosines of the normal to the preexisting plane by

$$\sigma_n = l'^2_n\sigma_1 + m'^2_n\sigma_2 + n'^2_n\sigma_3 \tag{7a}$$

$$\tau_n = \left[\left(l'^2_n\sigma_1^2 + m'^2_n\sigma_2^2 + n'^2_n\sigma_3^2\right) - \left(l'^2_n\sigma_1 + m'^2_n\sigma_2 + n'^2_n\sigma_3\right)^2\right]^{1/2}. \tag{7b}$$

Alternatively, the stress components on the preexisting planes can be related to the effective principal stresses and the pseudo-dip direction and pseudo-dip angle of the plane in the new coordinate system as

$$\sigma_n = \sigma_1\cos^2\varphi' + \sigma_2\sin^2\varphi'\cos^2\theta' + \sigma_3\sin^2\varphi'\sin^2\theta' \tag{8a}$$

$$\tau_n = \left[\left(\sigma_1^2\cos^2\varphi' + \sigma_2^2\sin^2\varphi'\cos^2\theta' + \sigma_3^2\sin^2\varphi'\sin^2\theta'\right) - \sigma_n^2\right]^{1/2} \tag{8b}$$

where $\theta'=\alpha'+90°$ in Fig. 1a, is the pseudo-dip direction and φ' is the pseudo-dip angle of the preexisting plane in the ($\boldsymbol{x'_1}$, $\boldsymbol{x'_2}$, and $\boldsymbol{x'_3}$) coordinate system. Pseudo-dip direction and dip angles θ' and φ' only become true dip direction and dip angle when the new coordinate axes ($\boldsymbol{x'_1}$, $\boldsymbol{x'_2}$, and $\boldsymbol{x'_3}$) are horizontal or vertical. From Eqs. (3) and (8a and b), we obtain the reactivation-tendency factor for the jth weak plane f_R^j in the ($\boldsymbol{x'_1}$, $\boldsymbol{x'_2}$, and $\boldsymbol{x'_3}$) coordinate as:

$$f_R^j = \frac{\tau_n}{\tau_n^j} = \frac{\left[\left(\sigma_1^2\cos^2\varphi' + \sigma_2^2\sin^2\varphi'\cos^2\theta' + \sigma_3^2\sin^2\varphi'\sin^2\theta'\right) - \sigma_n^2\right]^{1/2}}{C_W^j + \mu_W^j\sigma_1\cos^2\varphi' + \sigma_2\sin^2\varphi'\cos^2\theta' + \sigma_3\sin^2\varphi'\sin^2\theta'} \tag{9}$$

As f_R^j relates only to the effective principal stresses and the frictional properties on the plane, its physical meaning may be expressed graphically in the Mohr space. To illustrate this, we consider two preexisting planes having the same coefficient of friction but different cohesive strengths (i.e., $C_W>0$ and $C_F=0$) (Fig. 2). The pole of the preexisting plane, which is the same as the normal to the plane, is defined by its pseudo-dip direction and pseudo-dip angle of θ' and φ' in the Mohr space. The pole plots on the frictional strength line when its reactivation factor $f_R^W=1.0$ (line b in Fig. 2) and above the line when $f_R^W>1.0$. The sequence of weak-plane reactivation during a progressive decrease in the minimal compressive stress (σ_3), and thus an increase in the size (i.e., the radius) of the Mohr circle representing the stress state, can be predicted using the concept of reactivation-tendency analysis as shown in Fig. 2. The critical stress of the first weakness (P_1) was reached first while the other two weak planes (P_2 and P_3) remain stable (Fig. 2a). With a further decrease in the minimal stress, the second weakness plane (P_2) becomes activated when its critical shear stress is reached (Fig. 2b). Meanwhile, the third weak plane (P_3) remains stable. Finally, the critical stress for Coulomb fracturing is reached, which leads to the stabilization of the stress state but leaves the third weak plane (P_3) in a stable state (Fig. 2c).

3. Testing the model using a sandbox experiment

We test our simple mechanical model using a sandbox experiment (Fig. 3). The sandbox is 40 cm wide and 54 cm long in the plan view, which was filled by 8 cm thick dry quartz sand over an elastic rubber sheet at the base. The rubber sheet in turn was connected with a moving wall driven by motor (Fig. 3). The speed of the moving wall used in the experiment is 2 mm/min. Three preexisting weak planes (P_{w1}, P_{w2} and P_{w3}), oriented obliquely to the extension direction (i.e., the σ_3 direction), are implemented. The weak planes are made of thin sheets of regular printing papers with a coefficient of friction $\mu_w=0.36$. The dip angles of the weakness planes are the same at $\varphi_1=\varphi_2=\varphi_3=60°$. However, their dip directions differ, as $\theta_1=10°$,

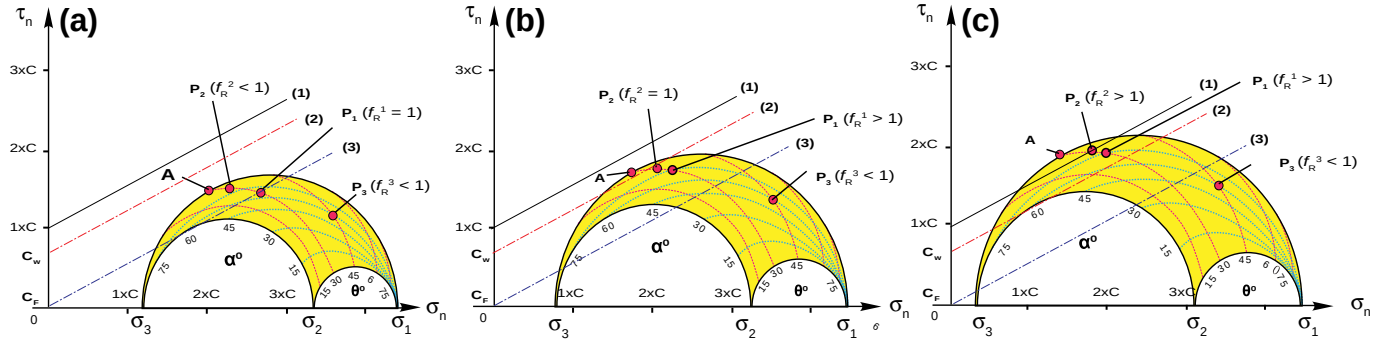

Fig. 2. Illustration of how the sequence of weak-plane reactivation during a progressive increase in the minimal compressive stress can be predicted using the concept of reactivation tendency (see the text for details). The magnitudes of principal stresses are scaled to the cohesive strength for coherent rock, C. Straight lines (1), (2) and (3) represent the Coulomb fracture envelop, the frictional strength envelop of the stronger preexisting plane, and the frictional strength envelop of the weaker preexisting plane. (a) The critical stress state of the first weakness (P_1) reactivating while other two weak planes (P_2 and P_3) remain stable. (b) The second weakness plane (P_2) is activated when its critical stress is reached. Meanwhile, the third weak plane (P_3) remains stable. (c) The critical stress of Coulomb fracturing was reached, which leads to the stabilization of the stress state, leaving the third weak plane (P_3) in a stable state.

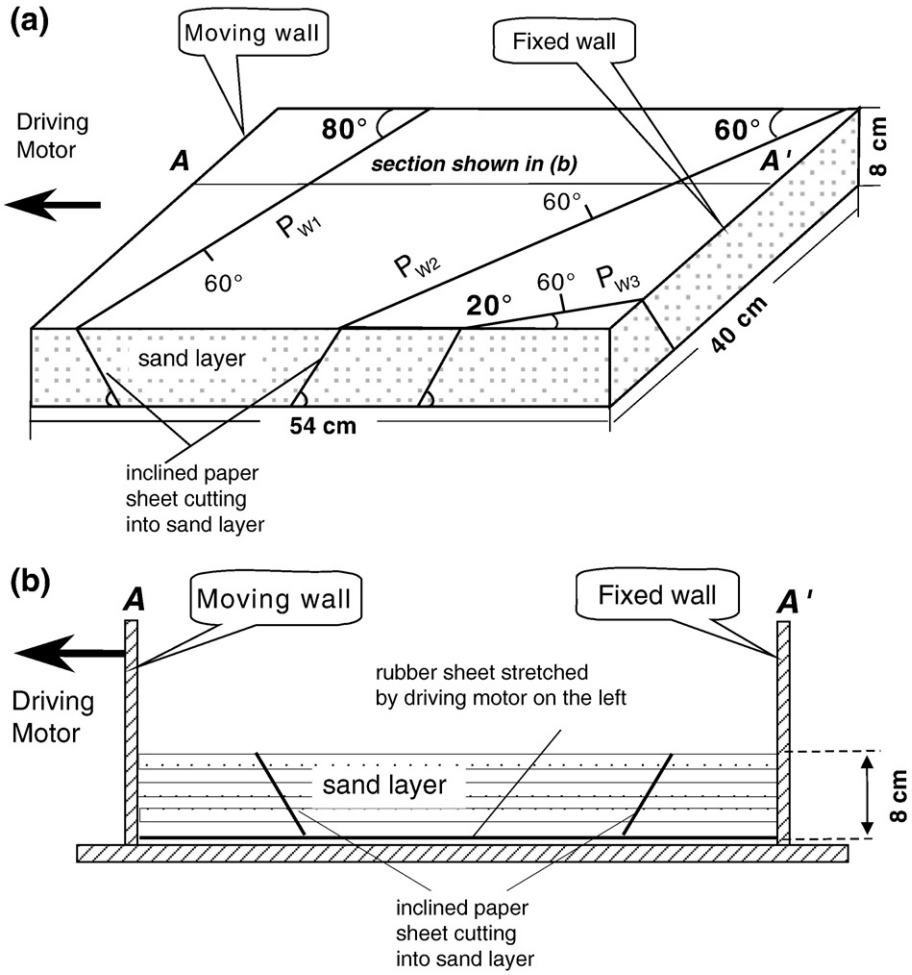

Fig. 3. (a) A sketch of the sandbox model design. P_{w1}, P_{w2}, and P_{w3} are preexisting weakness planes oriented obliquely to the extension direction: $\theta_1 = 10°$, $\theta_2 = 30°$, $\theta_3 = 7\ 0°$, $\varphi_1 = \varphi_2 = \varphi_3 = 60°$. AA′ shows the cross section of the sandbox shown in (b). A motor is linked with a rubber sheet at the base of the sand layer. The motor is also linked with the moving wall on the left side of the experimental apparatus. The right side of the wall is fixed.

$\theta_2 = 30°$ and $\theta_3 = 70°$, respectively (Fig. 4). As the friction angle (i.e., the angle of repose) of the dry quartz sand is ~31°, we assign its coefficient of friction to be $\mu = 0.60$. As the cohesive strength of dry sand is small (Adam et al., 2005; Eisenstadta and Simsb, 2005), we assume that it is negligible. Under this condition, the relative reactivation-tendency factors of the three weakness planes have the following relationships: $f_R^1 > f_R^2 > f_R^3$ (Fig. 4). Specifically, when the stress state is at the verge of Coulomb fracturing, we have $f_R^1 > f_R^2 > 1.0$ and $f_R^3 < 1.0$ (Fig. 4). The above relationship requires the following sequence of deformation: reactivation of weak planes 1 and 2 sequentially first, which is followed by the final development of Coulomb fractures, and weak planes 3 will keep inactive (Fig. 4). This prediction is verified by our sandbox experiment that simulated a progressive reduction of the minimal compressive stress during protracted extension (Fig. 5). Specifically, weak plane P_{w1} was reactivated first as a single fault (Fault No.① in Fig. 5a), which was followed by the formation of its antithetic and en echelon array faults (Fault No.② in Fig. 5b). Meanwhile, weak planes P_{w2} and P_{w3} remained inactive (Fig. 5a, 5b). As extension continued, weak plane P_{w2} became activated, forming an en echelon array of fractures along the preexisting weakness (Fig. 5b). At the same time, motion on P_{w1} continued. Further extension led to reactivation of weak plane P_{w2} (Fig. 5c), which was followed by the development of freshly created minor normal faults in a region between P_{w1} and P_{w2} (Fig. 5d). Note that P_{w3} remained inactive, as predicted by our reactivation tendency analysis. As the minor faults are oriented perpendicularly to the extensional direction, we interpret them to be Coulomb fractures with their formation unrelated to the reactivation of the preexisting planes. This evolutionary path of sequentially reactivating preexisting weakness and the final formation of the Coulomb fractures are consistent with predictions according to our reactivation-tendency analysis as shown in Fig. 4.

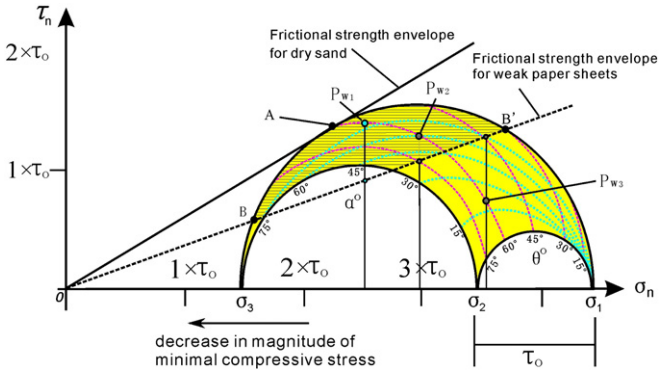

Fig. 4. A Mohr space diagram to illustrate the possible stress evolution of the sandbox experiment with the geometry of preexisting planes shown in Fig. 3. The magnitudes of principal stresses are scaled by $(\sigma_1 - \sigma_2)$. Points P_{w1}, P_{w2} and P_{w3} represent the pole positions of the three weakness planes defined by their trend and plunge. Point "A" represents the pole position of the freshly created Coulomb fractures and the stress circle reaches the fracture failure line.

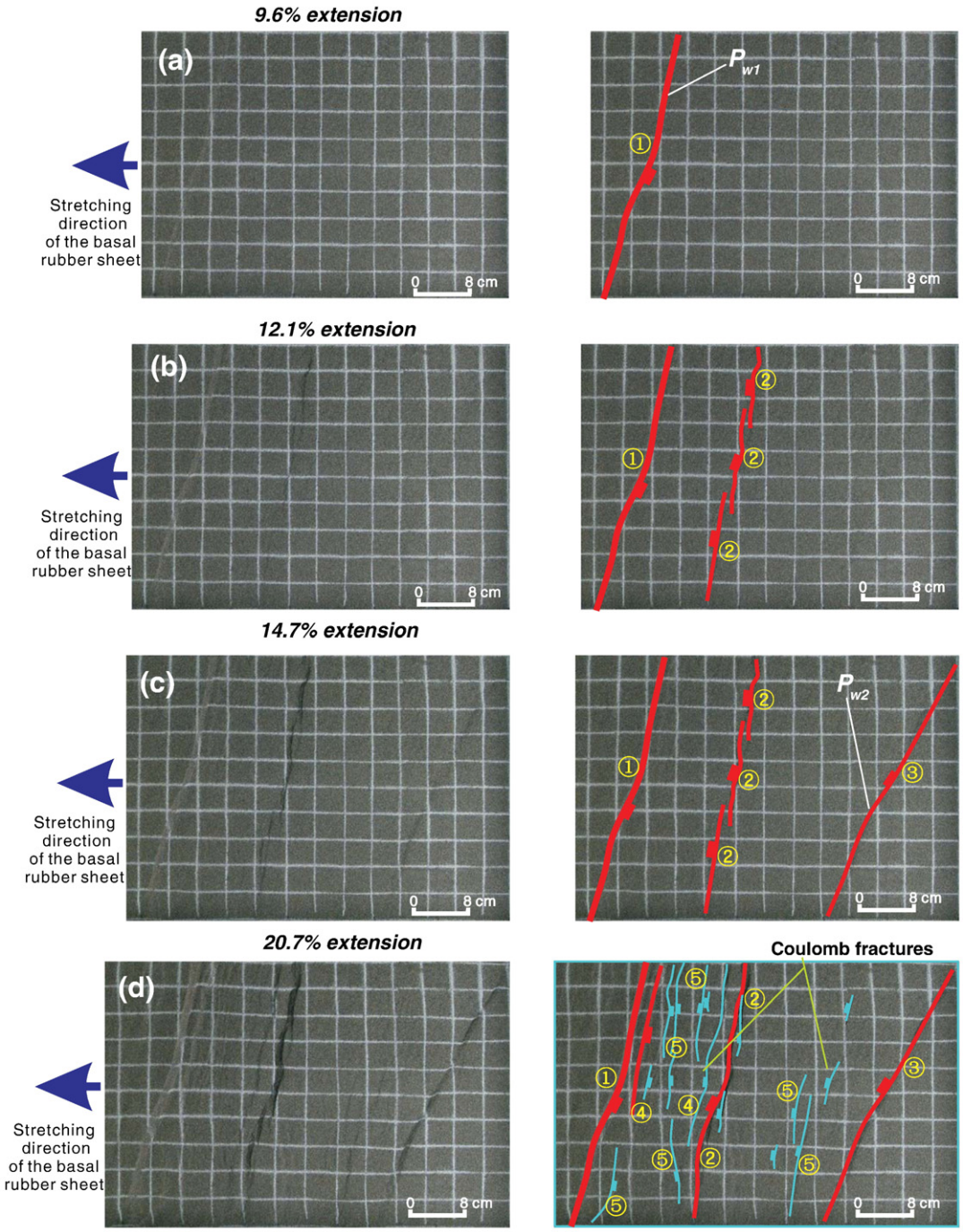

Fig. 5. Sandbox modeling results (left-column diagrams) and their structural interpretations (right-column diagrams). (a) P_{w1} was reactivated as a single fault while P_{w2} and P_{w3} remain inactive. (b) The antithetic faults of Pw1 reactivated fault began to form, P_{w2} became activated, forming an echelon array. Meanwhile, motion on P_{w1} continued. (c) P_{w2} became activated while motion on P_{w1} and P_{w2} was continuing. (d) Fresh minor normal faults between P_{w1} and P_{w2} were created; they are perpendicular to the extensional direction (i.e., the horizontal while lines in the grid) but oblique to the surface traces of P_{w1} and P_{w2}, while P_{w3} remained inactive as predicted. We interpret the minor normal faults them for have formed as Coulomb fractures unrelated to the reactivation of the preexisting planes. Also notice that minor fractures were created near weak plane P_{w3}. These fractures trend more northerly than P_{w3}, and thus were probably also created by Coulomb fracturing.

4. Discussion and conclusions

Although this study was fundamentally built upon the pioneer work of Morris et al. (1996), our newly defined *reactivation-tendency factor* and the underlying theoretically framework provide a much general treatment on the mechanical reactivation of preexisting weakness. Specifically, three early assumptions made in the Morris et al. (1996) analysis can now be removed: (1) uniform coefficient of friction on all preexisting planes, (2) negligible cohesive strength, and (3) principal stresses must be oriented vertically or horizontally. Using a coordinate-system transformation, we also developed a new graphical technique in expressing our general treatment of the reactivation problem in the Mohr space, which is familiar to most geologists. Finally, the predicted sequence of reactivation on pre-existing weakness and initiation of new fractures according to the Byerlee Law and the Coulomb fracture criterion were verified by a simple sandbox experiment.

A key assumption in both the slip-tendency analysis of Morris et al. (1996) and our reactivation-tendency analysis is that the preexisting weakness must be planar. This assumption, however, does not prevent

the application of the analysis developed in this study, as curved surfaces can always be divided into small segments of approximately planar elements. In this sense, our analysis can be expanded to evaluate the likelihood of future seismicity on different segments of a single fault with curvi-planar geometry. This approach may be particularly appropriate for listric normal faults, ramp-flat thrusts, and strike-slip faults with restraining- and releasing-bend geometry.

Another important assumption in our analysis is that the formation of fault zones and their activities do not affect the regional stress distribution. This assumption is clearly an oversimplification, as both detailed analysis of fault-zone evolution and regional modeling show that frictional sliding on faults is capable of creating stress fields near the faults that are significantly different from the regional stress field (e.g., Gudmundsson et al., 2010; Yin, 1994). In the Yin (1994) analysis, preexisting weak planes were treated as Coulomb materials embedded within a homogenous elastic plate under regional uniform stress. In contrast, Gudmundsson et al. (2010) considered preexisting weak zones as elastic inclusions with different elastic properties from those surrounding the weak zones. Both rheological models mentioned above differ from the physical processes we envisioned here, which is illustrated in our sandbox analog experiment. That is, we consider the coherent rock (i.e., sand in the experiment) and preexisting weak planes (i.e., papers embedded in the sand) are frictional materials, which is more consistent with the generally perceived rheological model for Earth's lithosphere (e.g., Chen and Molnar, 1983), with the shear strength of rocks increases downward as a function of an increasing depth (i.e., normal stress) in the upper crust. The results of our model imply that the effect of activating preexisting weakness is minimal in changing regional stress. Exactly which rheological model is more appropriate in treating the preexisting weakness probably depends on the spatial scale of the problem and the actual rock type involved in deformation. More research is clearly needed to address this problem.

Our model also does not consider possible complex interactions among cracks within individual faults or faults that lie near one another. As stress concentrates at crack tips, it is expected that complex stress fields can be induced by the presence of cracks under uniform regional stress (e.g., Gudmundsson et al., 2009). Thus, our model should be considered more as an idealized conceptual guide, which can only be used in realistic situations when the above factors are considered.

Despite the complexities discussed above, our analysis does provide a new insight into the mechanical control on the temporal evolution of pre-existing weakness in geologic records. In the past, geologists tend to relate each phase of deformation indicated by the initiation of a new fault trend as a result of a new stress regime. Our analysis suggests that in a region with a progressive increase in the magnitude of differential stresses while the directions of the principal stresses maintain the same, multiple phases of fault initiation with different trends can be generated. The sequence of reactivation of the preexisting weakness is predictable according to the orientations and mechanical properties of the weak planes as shown in our reactivation-tendency analysis. As the sequence of faulting is generally known in the geologic record, geologists may use this information reversely for assessing the mechanical properties of the preexisting weakness at the time of their reactivation.

Acknowledgements

We would like to thank Ming-Yang Wang and Hua-Wu Hao for drafting some of the figures presented in this paper and assistance in conducting the sandbox experiment. Critical and constructive review by Agust Gudmundsson is greatly appreciated. Useful suggestions by chief editor Fabrizio Storti also helped clarify the text of this paper. This work is funded by China Natural Science Foundation (Grant No. 40772086) and partially funded by the Tectonics Program, U.S. National Science Foundation.

References

Adam, J., Urai, J.L., Wieneke, B., Oncken, O., Pfeiffer, K., Kukowski, N., Lohrmann, J., Hoth, S., van der Zee, W., Schmatz, J., 2005. Shear localisation and strain distribution during tectonic faulting — new insights from granular-flow experiments and high-resolution optical image correlation techniques. J. Struct. Geol. 27, 283–301.

Agostini, A., Corti, G., Zeoli, A., Mulugeta, A., 2009. Evolution, pattern, and partitioning of deformation during oblique continental rifting: inferences from lithospheric-scale centrifuge models. Geochem. Geophys. Geosyst. 10 (11), Q11015. doi:10.1029/2009GC002676.

Bailey, W., Ben-Zion, Y., 2009. Statistics of earthquake stress drops on a heterogeneous fault in an elastic half-space. Bull. Seismol. Soc. Am. 99, 1786–1800.

Byerlee, J.D., 1978. Friction of rocks. Pure Appl. Geophys. 116, 615–626.

Chen, W.-P., Molnar, P., 1983. Focal depths of intra-continental and intraplate earthquakes and their implications for the thermal and mechanical properties of the lithosphere. J. Geophys. Res. 88, 4183–4214.

Donath, F.A., 1961. Experimental study of shear failure in anisotropic rocks. Geol. Soc. Am. Bull. 72, 985–990.

Dyksterhuis, S., Muller, R.D., 2008. Cause and evolution of intraplate orogeny in Australia. Geology 36, 495–498.

Eisenstadta, G., Simsb, D., 2005. Evaluating sand and clay models: do rheological differences matter? J. Struct. Geol. 27, 1399–1412.

Geza, W., van Wees, J.-D., Bada, G., van Balen, R.T., Cloetingh, S., Pagnier, H., 2004. Slip tendency analysis as a tool to constrain fault reactivation: A numerical approach applied to three-dimensional fault models in the Roer Valley rift system (southeast Netherlands). J. Geophys. Res. 109 (B02401), 1–16.

Geza, W., Michon, L., van Balen, R.T., van Wees, J.-D., Cloetingh, S., Pagnier, H., 2005. Pre-Neogene controls on present-day fault activity in the West Netherlands Basin and Roer Valley Rift System (southern Netherlands): role of variations in fault orientation in a uniform low-stress regime. Quatern. Sci. Rev. 24, 475–490.

Gudmundsson, A., Friese, N., Andrew, R., Philipp, S.L., Ertl, G., Letourneur, L., Thordarson, T., Self, S., Larsen, G., 2009. Effects of dyke emplacement and plate pull on mechanical interaction between volcanic systems and central volcanoes in Iceland. A. Studies in Volcanology: The Legacy of George Walker. Special Publications of IAVCEI, vol. 2. Geological Society of London, London, pp. 331–347.

Gudmundsson, A., Simmenes, T.H., Larsen, B., Philipp, S.L., 2010. Effects of internal structure and local stresses on fracture propagation, deflection, and arrest in fault zones. J. Struct. Geol. 32, 1643–1655.

Li, Y.G., Vidale, J.E., Day, S.M., Oglesby, D.D., Cochran, E., 2003. Postseismic fault healing on the rupture zone of the 1999 *M* 7.1 Hector Mine, California, Earthquake. Bull. Seismol. Soc. Am. 93, 854–869.

Loïc, D., Feigl, K.L., Komatitsch, D., Árnadóttir, T., Sigmundsson, F., 2008. Three-dimensional mechanical models for the June 2000 earthquake sequence in the south Iceland seismic zone. Tectonophysics 457, 12–29.

McKenzie, D.P., 1969. The relation between fault plane solutions for earthquakes and the directions of the principal stresses. Bull. Seismol. Soc. Am. 59, 591–601.

Melosh, J.H., 1990. Mechanical basis for low-angle normal faulting in the Basin and Range province. Nature 343, 331–335.

Moeck, I., Kwiatek, G., Zimmermann, G., 2009. Slip tendency analysis, fault reactivation potential and induced seismicity in a deep geothermal reservoir. J. Geophys. Res. 31, 1174–1182.

Morris, A., David, A.F., Henderson, B., 1996. Slip-tendency analysis and fault reactivation. Geology 24, 275–278.

Sokoutis, D., Corti, G., Bonini, M., Brun, J.P., Cloetingh, S., Mauduit, T., Manetti, P., 2007. Modelling the extension of heterogeneous hot lithosphere. Tectonophysics 444, 63–79.

Spencer, J.E., Chase, C.G., 1989. Role of crustal flexure in initiation of low-angle normal faults and implications for structural evolution of the Basin and Range province. J. Geophys. Res. 94, 1765–1775.

Vidale, J.E., Li, Y.G., 2003. Damage to the shallow Landers fault from the nearby Hector Mine earthquake. Nature 421, 524–526.

Wesnousky, S.G., 1999. Crustal deformation processes and the stability of the Gutenberg–Richter relationship. Bull. Seismol. Soc. Am. 89 (4), 1131–1137.

Yin, A., 1989. Origin of regional, rooted low-angle normal faults: a mechanical model and its tectonic implications. Tectonics 8, 469–482.

Yin, A., 1994. Mechanics of monoclonal systems in the Colorado plateau during the Laramide orogen. J. Geophys. Res. 99, 22043–22058.

Yin, A., Kelty, T.K., 2000. An elastic wedge model for the development of coeval normal and thrust faulting in the Mauna Loa-Kilauea rift system in Hawaii. J. Geophys. Res. 105 25,909-25,925.